STM JOURNALS

Journal of
Polymer & Composites

https://journals.stmjournals.com/jopc

ISSN: 2321-2810 (Online)
ISSN: 2321-8525 (Print)
Volume 12, Special Issue 8, 2024
DOI (Journal): 10.37591/JoPC

Research JoPC

Analyzing Cavitation in Marine Propeller: A Computational Approach with Consideration for Polymer Applications

Nikhil Babu P.[1]*, T.J.S. Jothi[2], Jaison Cletus[3], A.V. Ramesh Kumar[4]

Abstract

A major source of noise and blade damage in marine propellers is because of the phenomenon of hydrodynamic cavitation. The Computational Fluid Dynamics (CFD) analysis approach is employed for the prediction of the cavitating propeller's performance characteristics under various conditions of operation with the advance coefficient (J) ranging from 0.55 to 0.91 and cavitation number (σ) in the range of 0.80 to 4.50. The numerical simulation is performed on INSEAN E779A propeller model with diameter, D = 0.227 m (radius, R = 0.1135 m). The results of torque coefficient (K_Q), thrust coefficient (K_T) and open water efficiency (η) are compared with open water characteristics and found that the relative error is ≤ 10% for K_Q, and ≤ 15% in cases of K_T and η. The vapor volume fraction and static pressure contours are employed to visualize the extent of cavitation. The maximum volume fraction distribution is observed to be 72% along the chord length of 0.7R. Similarly, the maximum velocity is found to be 42.5 m/s for the operating condition of J = 0.55 and σ =0.80. The determination of these maximum extends is performed in order to determine the areas on propeller surface for applying suitable polymer coatings for cavitation mitigation. Finally, from the acoustic analysis, it is identified that the Sound Pressure Level (SPL) is higher when the propeller operates at J = 0.55 and σ = 0.80. The average increase in the overall Sound Pressure Level (SPL) is 21.23 dB between the two extreme cases, (a) case 1: J = 0.91 and σ = 4.50, and (b) case 6: J = 0.55 and σ = 0.80.

Keywords: Marine propeller, Hydrodynamic cavitation, Propeller performance, *INSEAN* E779A, cavitation number, acoustic analysis, numerical simulation

INTRODUCTION

Hydrodynamic cavitation will be initiated when the local pressure is reduced below the vapor pressure of the liquid at that particular temperature [1]. This process is rather a complex process as it involves the effects of operating conditions, the quality of water and geometry of the propeller blade. Several negative effects may be linked to it, depending on the type of cavitation (tip vortex, sheet, cloud, bubble, etc.). These include shaft vibration and performance loss, increasing the drag force of rotating parts, and mainly erosion of the blade caused by imploding cavities close to the blade surfaces. The marine propeller's radiated noise level will also be significantly raised.

For the reliable operation of onboard acoustic instruments, naval or research vessels must be designed to minimize underwater noise radiated from the vessel. According to Ross [2], machinery,

*Author for Correspondence
Nikhil Babu P.

[1]Research Scholar, Department of Mechanical Engineering, NIT Calicut, Kerala and Naval Physical and Oceanographic Laboratory (NPOL), Kochi, Kerala, India
[2]Associate Professor, Department of Mechanical Engineering, NIT Calicut, Kerala, India.
[3]Scientist 'E', Naval Physical and Oceanographic Laboratory (NPOL), Kochi, Kerala, India.
[4]Scientist 'G', Naval Physical and Oceanographic Laboratory (NPOL), Kochi, Kerala, India

Received Date: March 21, 2024
Accepted Date: July 12, 2024
Published Date: October 23, 2024

Citation: Nikhil Babu P., T.J.S. Jothi, Jaison Cletus, A.V. Ramesh Kumar. Analyzing Cavitation in Marine Propeller: A Computational Approach with Consideration for Polymer Applications. Journal of Polymer & Composites. 2024; 12(Special Issue 8): S29–S44p.

propellers, and background hulls are the main contributors to underwater noise. Noise from cavitating propellers can span a large frequency range and is dangerous during acoustic survey operations, according to Sasajima et al. [3].

The propeller's performance is examined in terms of certain parameters, such as thrust coefficient (K_T), torque coefficient (K_Q) and the open water efficiency (η), which are given by Eqs. 1-3:

$$K_T = \frac{T}{\rho n^2 D^4} \quad (1)$$

$$K_Q = \frac{Q}{\rho n^2 D^5} \quad (2)$$

$$\eta = \frac{K_T}{K_Q}\frac{J}{2\pi} \quad (3)$$

Where, J is advance coefficient, defined as in Eq. (4):

$$J = \frac{V_a}{nD} \quad (4)$$

Another parameter influencing the hydrodynamic cavitation is the cavitation number (σ) given by Eq. (5):

$$\sigma = \frac{P_\infty - P_V}{\frac{1}{2}\rho(nD)^2} \quad (5)$$

These open water characteristics are employed to predict the extent of cavitation on the propeller surface. The prediction of cavitation in various marine systems began with the usage of lifting line theory, with the blade represented by a vortex line and the wake by helicoidal vortices. Numerical models quickly advanced, beginning in the 1960s. Salvatore et al. [4] employed perturbation methods to describe the lifting-line theory theoretically. In order to determine the flow pattern and performance parameters of a DTNSRDC P4119 marine propeller in a uniform flow, Chang [5] used a finite volume CFD method in conjunction with the common k-turbulence model. A numerical analysis on hydrodynamic and hydroacoustic performance of a cavitating marine propeller in open water condition using Reynolds-averaged Navier-Stokes (RANS) and Detached Eddy Simulation solvers was performed by Savas Sezen [6]. They investigated the effectiveness of both these methods and found that both could be used for modelling sheet cavitation in marine propellers. An investigation was numerically performed by Salvatore et al. [7], utilizing the *INSEAN*-PFC propeller flow code created by CNR-*INSEAN*. The open water performance, the assessment of the velocity field in the wake of the propeller, and the prediction of cavitation under uniform flow circumstances are all studied through experiments. The hydrodynamic characteristics of pump-jet under cavitating flow conditions were studied with RANS using structured grid, SST k−ω turbulence model by Pan et al. [8]. The simulation could predict the cavitation inception on the rotor's suction side accurately. An experimental and theoretical examination of a cavitating propeller with uniform inflow was provided by Pereira et al. [9]. To provide quantitative statistics on the cavity extension, studies were performed on flow field by utilizing the advanced imaging techniques. Multiple studies are conducted in the field to reduce cavitation by applying polymer coatings on the surface of the propeller [10]. Theoretical research suggests that underwater sound absorption materials must adhere to two crucial principles: (a) The characteristic impedance should be in line with the impedance of water in order to minimize the reflection of incoming sound waves, and (b) the materials used should have high enough attenuation qualities to effectively absorb the sound waves that pass through them [11]. Since most polymer materials have good damping qualities and a close acoustic impedance with water, they form the basis of most underwater sound absorption materials. Polymer materials also offer very good resistance to corrosion, water, heat, ozone & oxidation, good thermal and electrical insulation properties, low cost, and simple manufacture, which makes them ideal for underwater applications [12–14]. The polymer coating system, having high bonding strength to the surface of the propeller, can be a good solution that can help delaying cavitation phenomenon and reduce cavitation noise. But the major concern would be the identification of the areas on the propeller surface requiring the polymer usage. This has to be identified using numerical simulations before experimenting with the same.

The turbulent vorticity-confinement approach was developed by Pereira and Sequeira [15] for RANS-based industrial propeller-flow simulations. The approach seeks to enhance the prediction of cavitation-causing tip vortices. Several scholars have used an equation predicting single bubble dynamics, that is, the, Rayleigh-Plesset equation, as the basis for modelling cavitation. Schnerr and Sauer [16] added a link between the bubble nuclei and volume fraction in the Rayleigh-Plesset equation to create a cavitation model. By making a suitable prediction of cavitation inception around the nozzle neck, they validated their model. In view of dealing with the viscous flows, several researchers have numerically predicted cavitation based on RANS models, which are considered as the relevant area of research. Maksoud [17] and Watanabe et al. [18] were able to generate the first simulation results using RANS in marine propellers under cavitation. They observed that the flow was severely influenced by the local flow velocity and the pressure conditions. The "*INSEAN*" propeller flow code was used to perform computational predictions by Salvatore et al. [7]. Additionally, tests were done to verify the cavitation under uniform flow prediction. A cavitating propeller in a uniform inflow was the subject of experimental and theoretical research by Pereira et al. [9]. Quantitative data on the cavity's size was obtained using advanced imaging techniques.

As cavitating flows involve both liquid and vapor phases and both phases are in equilibrium, the multiphase flow system is assumed to be homogeneous, and each phase is acted upon by same velocity and pressure fields. The RANS formulation with certain modifications is employed for solving the multiphase flow problems.

The equation of continuity for this flow is given as:

$$\frac{\partial}{\partial t}(\rho_m) + \nabla.\left(\rho_m \vec{V}_m\right) = 0 \tag{6}$$

The momentum equation is represented as:

$$\frac{\partial}{\partial t}\left(\rho \vec{V}_m\right) + \nabla.\left(\rho \vec{V}_m \vec{V}_m\right) = -\nabla p + \nabla.\left[\mu_m\left(\nabla \vec{V}_m + \nabla V_m^T\right)\right] + \rho_m \vec{g} + \vec{F} \tag{7}$$

This is the multiphase RANS equation with LHS corresponding to changes in mean momentum of an element of fluid caused due to flow unsteadiness occurred by convection in the mean flow. The additional modelling essential for the conventional single-phase RANS equation for performing this multiphase application is done using various turbulence models.

Now, in the acoustic context, the Lighthill equation, developed using the continuity and momentum equations in the acoustic setting, now serves as the fundamental equation for sound propagation [19]. The Lighthill equation [20] has a solution known as the Ffowcs Williams & Hawkings (FW-H) equation, and SPLs in the flow domain were extracted from the Finite Volume Method (FVM) using the FW-H formulation. A technique based on the FW-H equation and its integral solutions is provided by ANSYS Fluent software. Seol et al. [21] presented a study on non-cavitating underwater propeller noise in 2002 [22] and in 2005. They described the use of a hybrid method to predict underwater propeller noise in non-cavitating and cavitating conditions. They examined a DTMB4119 model, and the outcomes were reported for a low frequency range and only one operating condition. Bagheri et al. [23] conducted research on two marine propeller models in uniform flow and analyzed the acoustic and flow hydrodynamics. The sheet cavitation on propeller surface was examined and the study on acoustic effects of cavitation was performed. Through the FW-H equation, Pan et al. [24] also assessed the marine propeller noise in non-uniform flow in 2013. The FW-H equation can be evaluated in different ways. The FW-H equation was solved by utilising the panel approach in few works [21–24]. Various studies have been performed using commercial codes like CFD and Fluent software. They extracted the SPLs by flow field analysis using the RANS equation solver.

The numerical investigations in this paper are performed on *INSEAN* E779A model propeller, which is an old designed four bladed fixed pitched propeller. This small skewed propeller was designed in 1959 and was tested by *INSEAN* (Instituto Nazionale di Studi ed Esperienze di Architettura Navale) in various non cavitating and cavitating conditions for numerous research and experimental studies.

It is clear from all the above literatures that researchers have done numerous studies towards the prediction of cavitation in marine propellers. However, these works did not make a considerable investigation on the distribution of vapor volume fraction as well as flow velocity past the propeller blade surface, which are the major contributing factors for cavitation. Further, the acoustic analysis was not numerically predicted for the *INSEAN* propeller, which is actually an ideal model propeller that can be utilized for predicting cavitation characteristics under a given condition and can be practically extrapolated to real propellers. Moreover, in this study, the distribution of vapor volume fraction and velocity, both by visualization and quantitative mode, over the propeller surface at 0.7R is carried out. The acoustic analysis is also performed for both extreme cases, which are (a) case 1: J = 0.91 and σ = 4.50, and (b) case 6: J = 0.55 and σ = 0.80, by adopting four receivers and predicting the SPL over the frequency range.

Hence, the three-dimensional, viscous, uniform, and cavitating flow of *INSEAN* E779A model propeller is simulated using ANSYS Fluent CFD software. In order to estimate the overall SPLs in this study, the flow field was first analysed using the Finite Volume Method (FVM). The flow data, which included pressure variations, cavitation volume, and results of the velocity magnitude of the flow solution, were then used as inputs for the Ffowcs Williams & Hawkings (FW-H) formulation for the prediction of overall SPL.

COMPUTATIONAL METHODOLOGY

The ANSYS Fluent CFD software [25] is employed for the analysis of hydrodynamic and acoustic characteristics. '*INSEAN* E779A' propeller model is used for analysis purposes and the details of its geometry are listed in Table 1. The geometry of the same is generated from the 'HYDROCOMP PROPCAD' software (Figure 1). The fluid domain is considered continuum, and the properties of water and water vapor are assigned as it is a multiphase phenomenon.

Computational Domain and Mesh Generation

The three-dimensional computational domain is created using the Design Modeler feature in ANSYS Fluent software.

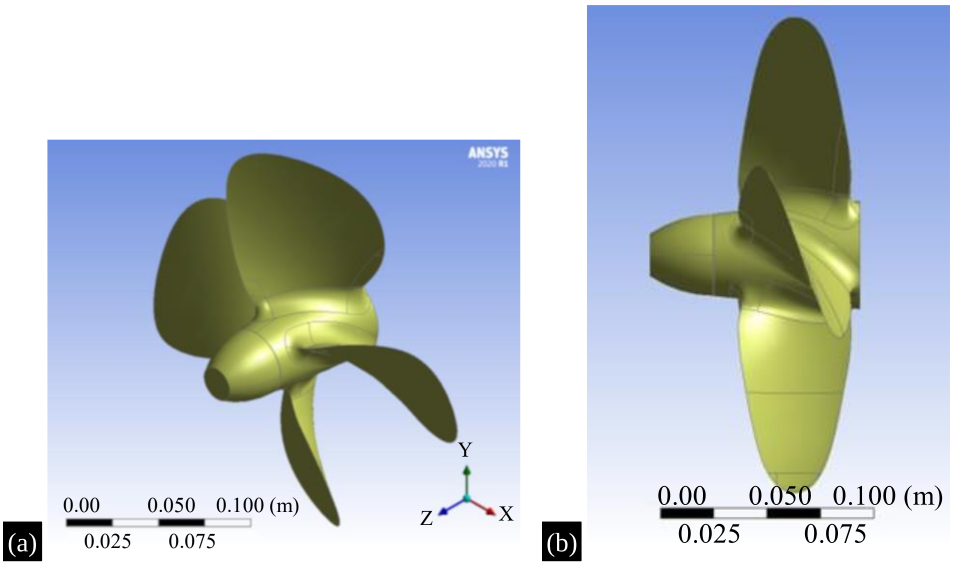

Figure 1. *INSEAN* E779A Propeller model.

Figure 2 shows the computational domain used for the purpose of simulation. The entire domain is divided into a stationary domain and a rotating domain. The stationary domain has a diameter of 6*D* and a length of 10*D*, whereas the rotating domain is also a cylindrical enclosure over the propeller with a diameter of 1.1*D* and a length of 0.6*D*. The domain is extended up to 4*D* upstream and 6*D* downstream of the propeller. The Mesher package in the software is used for discretization of the computational domain into meshed elements. Unstructured tetrahedral meshing is being adopted for the analysis as shown in Figure 2 (c). For obtaining the effects of the boundary layer on the propeller blade walls, prismatic inflation layers (inflation layers: 20, growth rate: 1.2) are provided. The element size is 0.04 m with a maximum size of 0.12 m. A grid independence test was carried out in order to ensure the accuracy of the results generated during the analysis, which is described in the next section. For the purpose of predicting flow around the propeller, the fluid is assigned a Moving Reference Frame (MRF).

Table 1. Propeller geometry details.

***INSEAN* E779A Propeller**	
Diameter of the Propeller (*D*)	0.227 m
Blade number	4
Pitch ratio	1.1
Skew angle at blade tip	4^o 48’ (positive)
Rake (nominal)	4^o 35’ (forward)
Expanded area ratio	0.689
Hub diameter	0.045 m
Hub length	0.098 m

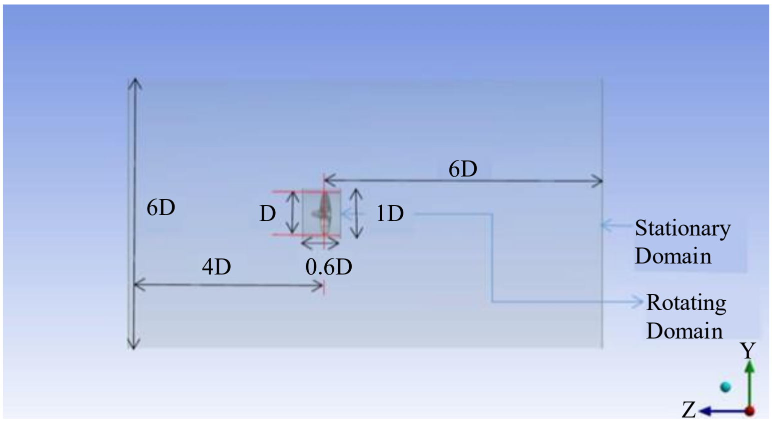

(a)

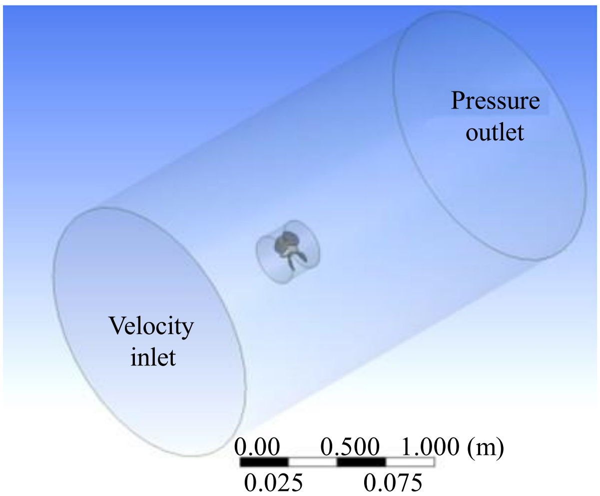

(b)

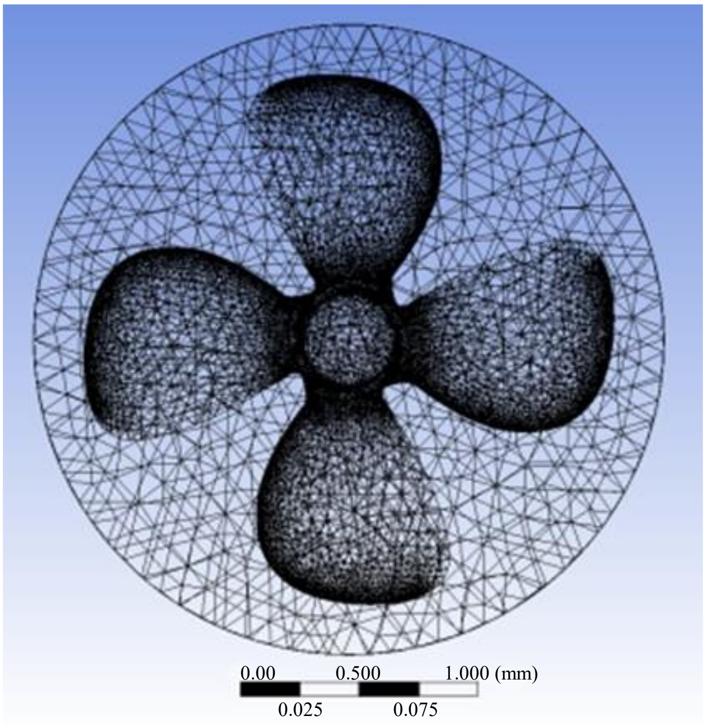

(c)

Figure 2. (a) Computational domain with dimensions (b) Isometric view of the domain (c) Meshed propeller and rotating domain.

Boundary Conditions

The fluid inlet velocity (V_a) and outlet pressure data are given to the solver as per the parameters given in Table 2. The propeller surface, consisting of the blade and the hub, was assigned zero rotational velocity relative to the adjacent cell zone. Also, the far-field boundary was set at an absolute rotational velocity of zero and was taken as an inviscid wall. The simulation involves preliminary conditions such as pressure-based transient multiphase modelling with realizable k-ε turbulence viscous modelling. The multiphase interaction was supplemented with a mass transfer model, as cavitation involves interphase mass transfer. Hence, the Schnerr-Sauer model is adopted as the cavitation model.

Numerical Schemes and Convergence

The pressure-velocity coupling was solved using the 'SIMPLE' technique. The Least Squares Cell Based method is employed for the gradient discretization. Pressure interpolations were given as 'PRESTO' and a second-order upwind scheme was used in the spatial discretization of momentum, turbulent kinetic energy, and turbulent dissipation rate. Then, the source and the receivers are assigned to solve the FW-H sound equation. The convergence criteria were set at 10^{-5} for all the residuals. It is crucial to minimize round-off, iterative convergence and discretization errors in every CFD investigation. By using double precision, round-off error has been reduced. The truncation criterion for all the residuals, which in this case is 10^{-5}, has been used to measure the iterative convergence error. Systematic space mesh refining is done to measure and lessen the discretization error.

For the present study, grid convergence studies were carried out for case 2 (J = 0.83, σ = 2.06) with various mesh sizes, and the results are as shown in Figure 3. The analysis was done to balance the computation time and accuracy for the value of the thrust coefficient (K_T). The optimum computational time was about 6 hours, and the optimum relative error % (R. error %) was 3.3319%. The corresponding grid numbers were of the order of 18 lakhs. But as the grid size for Large Eddy Simulation (LES) should be small enough in order to perform the acoustic simulations, the optimum was selected to be slightly away from the obtained, that is, the grids of the order of 20 lakhs, with a computational time of 7 hours and R. error % of 3.1579% was selected, with a mesh size of 0.030 m.

Table 2. Flow parameters.

Case	*n (rpm)*	V_a *(m/s)*	*J*	*σ*
1	1500	5.10	0.91	4.50
2	1800	5.65	0.83	2.06
3	2000	6.00	0.80	2.00
4	2400	6.99	0.77	1.78
5	3000	8.00	0.71	1.76
6	5000	10.4	0.55	0.80

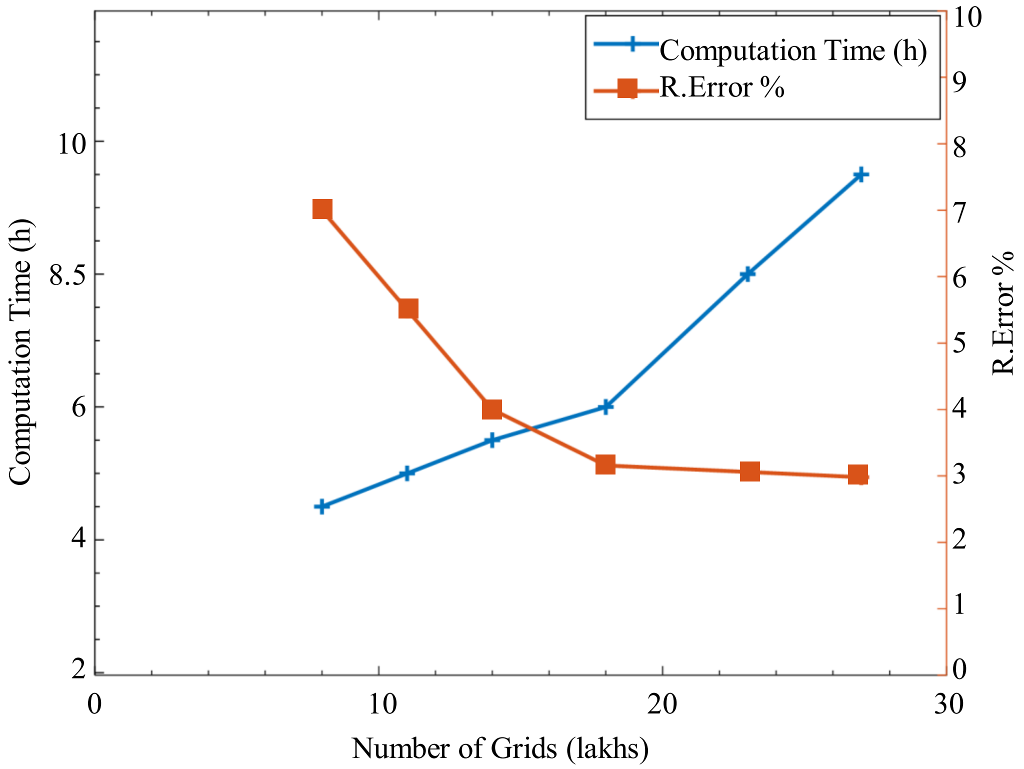

Figure 3. Grid independence study.

RESULTS AND DISCUSSION

The simulations were performed based on the flow parameters and conditions as per Table 2, and the extent of cavitation was observed in terms of the volume fraction of the vapor formed over propeller blade surface. The validation of the open water characteristics and their effect on cavitation numbers are investigated. The vapor volume fraction and velocity distribution over the propeller surface were quantified. The SPLs for the two extreme cases were also determined.

Validation of Open Water Characteristics

The CFD computations are carried out on the *INSEAN* E779A propeller model, and the results are validated with experimental data sets [9]. K_T, K_Q and η are given as in equations (1), (2), and (3), and the variation of the same with J is shown in Figure 4. The relative error percentage (R. error %) of K_T, K_Q and η are calculated using Eq. 8.

$$R.error\ (\%) = \frac{EXP\ results - CFD\ results}{EXP\ results} \times 100 \tag{8}$$

From Table 3, it is observed that the R. error % is less than 10% for K_Q, and the experimental values are higher than the CFD values. But in the case of K_T and η, CFD values are higher than the experimental values for lower values of J and σ. The R. error % are in the range below 15%.

Table 3. R. error % of open water characteristics.

Case	J	σ	R. error % of K_T	R. error % of K_Q	R. error % of η
1	0.91	4.50	9.0226	-5.8291	14.034
2	0.83	2.06	3.1579	-2.8947	5.882
3	0.80	2.00	4.7619	-5.0000	9.297
4	0.77	1.78	5.4167	-9.3023	13.466
5	0.71	1.76	-9.2308	-8.2677	-0.890
6	0.55	0.80	-10.1040	-9.1493	-0.403

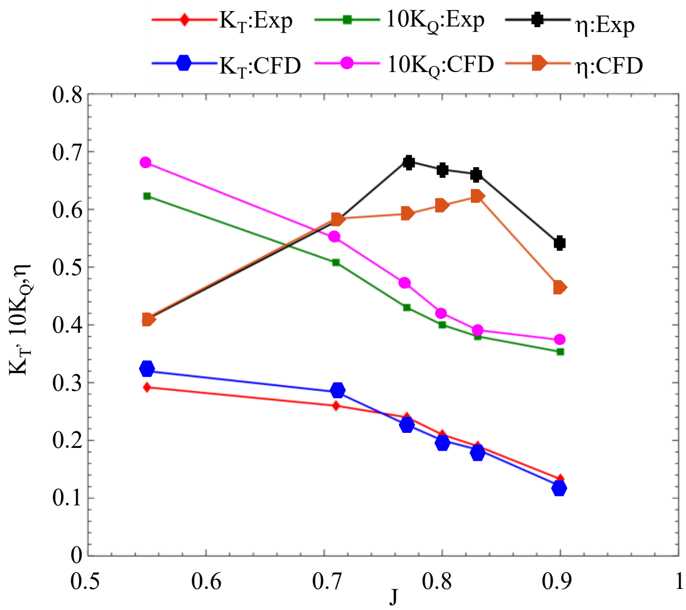

Figure 4. Comparison of performance characteristics.

Visualization of Cavitation

The phenomenon of cavitation can be accounted for by considering the vapor volume fraction on the propeller blade and static pressure distribution. Figure 5 shows the static pressure gradient over the propeller and fluid domain for case 5 with J = 0.71, σ = 1.76, and advance velocity, V_a = 8 m/s. The negative pressure regions are largely observed TO the suction side of the propeller in comparison to the pressure side. A large pressure gradient is also observed on the suction side due to the larger velocity of uniform free stream flow. The tip vortex cavitation is expected to occur at r/R = 1, where the static pressure shows a negative value, as observed in Figure 5. From Figure 6, the vapor volume is clearly visible on the leading edge of the blade surface on the suction side. It is observed that the vapor volume fraction zone increases from case 1 to case 6 in a gradual manner. This signifies the development of cavitation and its extension on the propeller surface. Thus, the area of application of polymer [26] coatings for its mitigation is also towards the leading-edge portion and extending towards the propeller tip.

Figure 7 represents the static pressure distribution on the surface of the propeller. The cavitation extent increases as the values of J and σ are reduced from case 1 to case 6. This condition occurs because a lower value of J implies higher rotational speeds of the propeller, and thus leading to propeller cavitation. Also, lower values of the cavitation number imply a larger extension of cavitation. Here, the extent of cavitation can be observed in terms of low-pressure zones (represented by dark blue shades), and these zones are gradually increasing on the propeller blade surface at the suction side, denoting an increasing order of cavitation from case 1 to case 6. From these contours as well, we could estimate the area on the propeller surface where the polymer coatings [27] need to be applied for mitigation of cavitation.

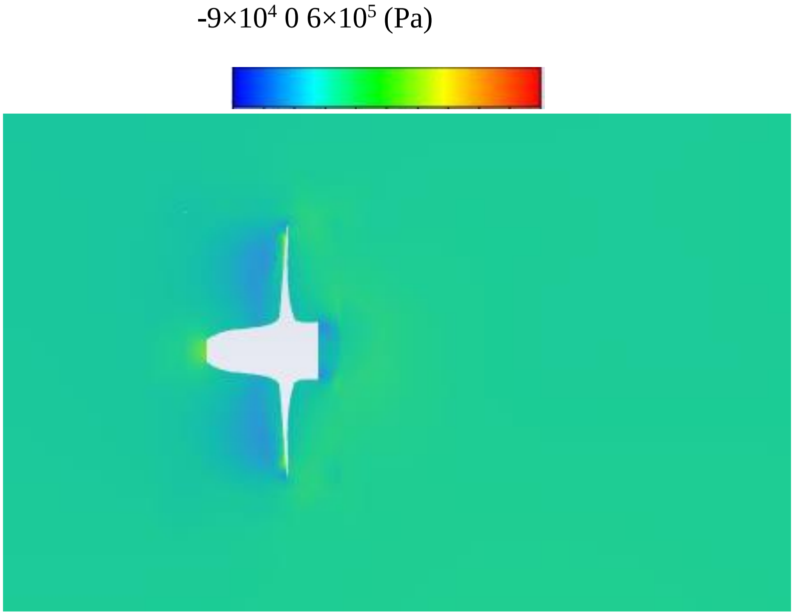

Figure 5. Static Pressure contour over the propeller and fluid domain.

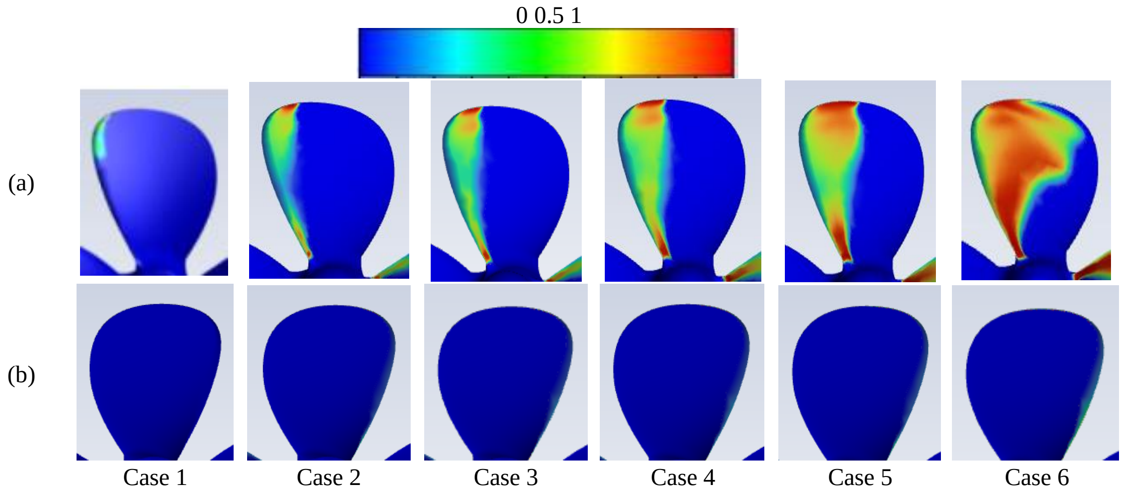

Figure 6. Vapor volume fraction contour (a) suction side and (b) pressure side.

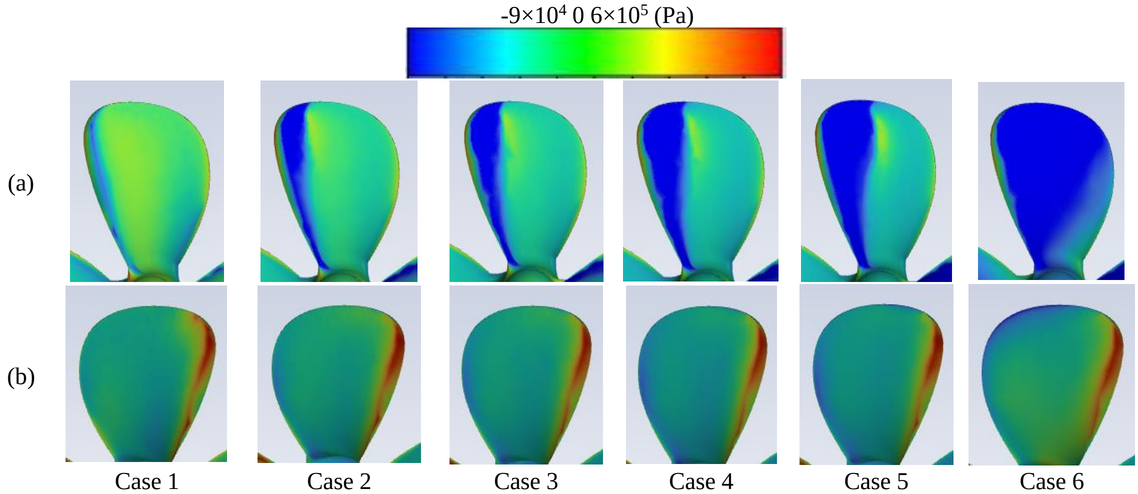

Figure 7. Static pressure distribution contour (a) suction side (b) pressure side.

Variation of Vapor Volume Fraction and Velocity Along the Chord Length

The accurate prediction of volume fraction distribution of the vapor phase and thereby cavitation area damage analysis is crucial from the perspective of mitigation of cavitation damage in a marine propeller. As depicted from the visualization plots, case 6 has the maximum distribution of vapor volume fraction in comparison to all other cases, as it corresponds to heavily cavitating case. But the vapor distribution varies along the radial distance on the propeller blade surface. For the calculation purposes in marine propeller analysis, attention is given to the analysis of the propeller blade surface for a radial distance of r/R = 0.7. Hence, the variation of vapor volume fraction on the propeller surface (suction side) at 0.7R is shown in Figure 8.

It is observed that there is no specific pattern in the distribution of vapor volume fraction. As the cavitation is observed near the tip portion on the suction side, the vapor volume fraction is mostly concentrated towards the leading-edge portion of the propeller blade. Hence, for most of the cases (case 1 to case 5), the vapor volume fraction distribution nearly approaches zero at the center of the propeller. In case 6, the vapor volume fraction is covering more than the mid-chord region, thereby, the distribution is seen to be different from the other cases. The maximum value is observed to be 72% at +0.02215 m from the reference line in case 6. Here, the '+' sign denotes the measurements made in the negative x direction from the reference (shown in Figure 1). Figures 9 and 10 denote the velocity contours over the propeller surface for case 5, with J = 0.71, σ = 1.76 and advance velocity, V_a = 8 m/s. The propeller blade experiences a wide gradient of velocity from its centre to the tip region. The maximum velocity was obtained to be of the order of 38.5 m/s. The maximum velocity zones and the pathlines of flow are also observed on the rotating domain, as shown in Figure 9.

The variation of velocity magnitude is also presented for r/R = 0.7 in Figure 11. The velocity magnitude almost remains constant at a particular radial distance in the rotating propeller system. But as the blade is curved, the variation of velocity along the chord length slightly increases towards the propeller edges. The velocity distribution has its peak at +0.041596 m, and the value is found to be 42.5 m/s for case 6. The average velocity from case 1 to case 6 over the entire chord length for 0.7R are 15.407 m/s, 16.812 m/s, 18.717 m/s, 22.204 m/s, 26.307 m/s, and 40.850 m/s, respectively.

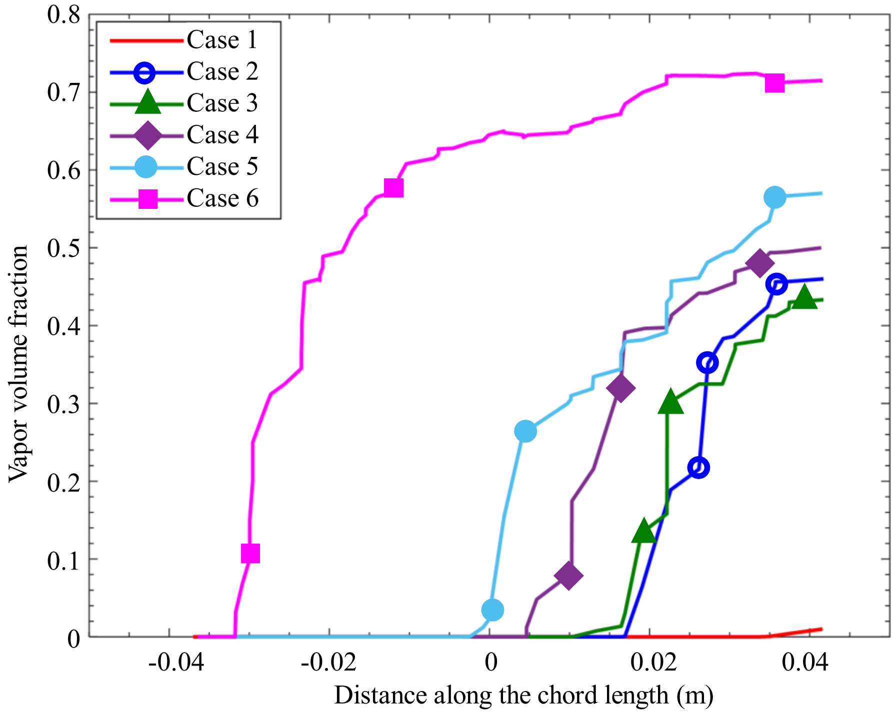

Figure 8. Distribution of vapor volume fraction at 0.7R.

Journal of Polymer & Composites
Volume 12, Special Issue 8
ISSN: 2321-2810 (Online), ISSN: 2321-8525 (Print)

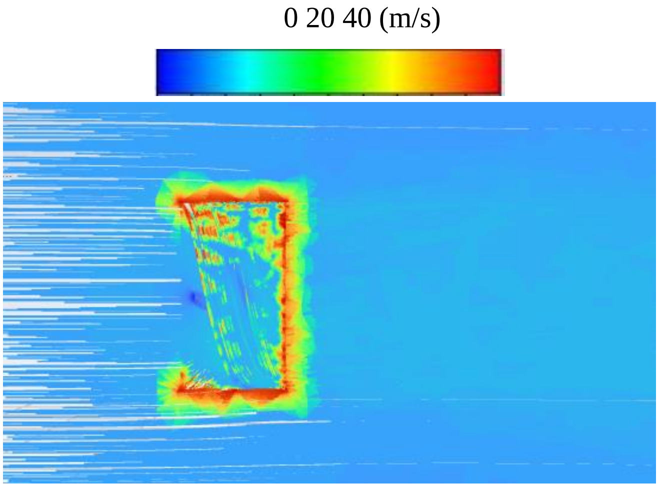

Figure 9. Pathlines of flow velocity along the propeller and rotating domain for case 5.

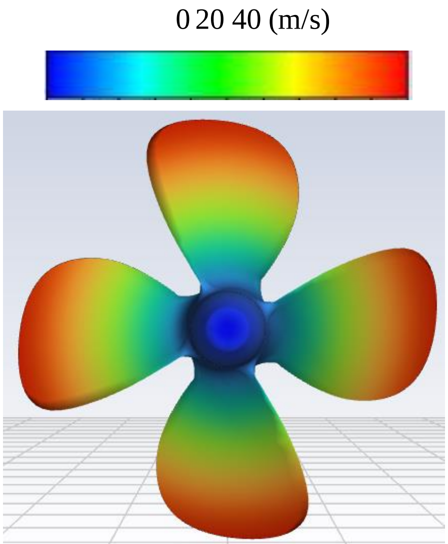

Figure 10. Velocity magnitude distribution over the propeller blade surface for case 5.

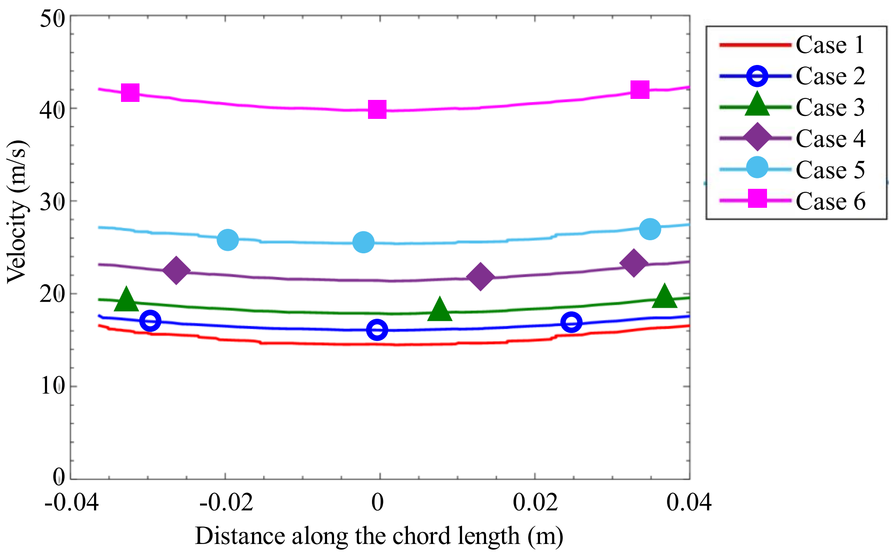

Figure 11. Distribution of velocity magnitude at 0.7*R*.

Acoustic Analysis

The results of the flow field are employed as the input value in the FW-H solution of Fluent software. For the same, the simulation is carried out by employing Large Eddy Simulation (LES), and the acoustic model is turned on for FW-H model. The acoustic source data is exported, and the corresponding model parameters are selected. This also involves defining the sources and receivers. The source zone is selected as the propeller surface. The selection of receivers involves determining its number and selecting the suitable coordinates for each receiver. The acoustic source data files are read by selecting the previously selected active source zones and receivers. The solution is computed based on all the source data files available.

In the analysis part, the effect of cavitation on the overall Sound Pressure Level (SPL) is investigated. The SPLs are generated for both the extreme cases: case 1 (J = 0.91, σ = 4.50) and case 6 (J = 0.55, σ = 0.80). Case 1 represents the condition of cavitation inception, and case 6 represents the state of larger cavitation extent as seen from visualization contours in Figure 6 and Figure 7. In this analysis, four receivers are employed to measure the overall SPL for the acoustic computations. The positions of the receivers (the marked positions are "not to scale") are shown in Figure 12. Figures 13 and 14 represent the spectrum of noise levels over the frequency range of the simulation for case 1 and case 6 respectively.

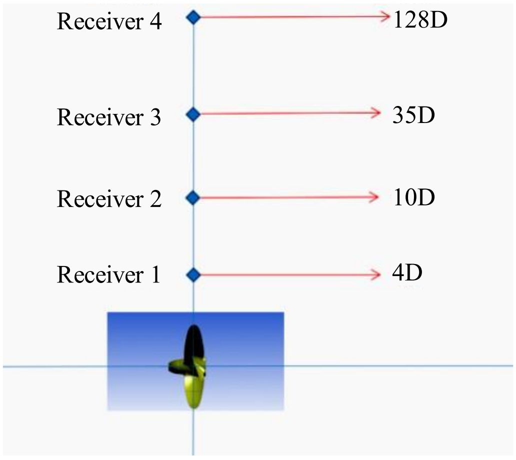

Figure 12. Receiver Positions along Y axis.

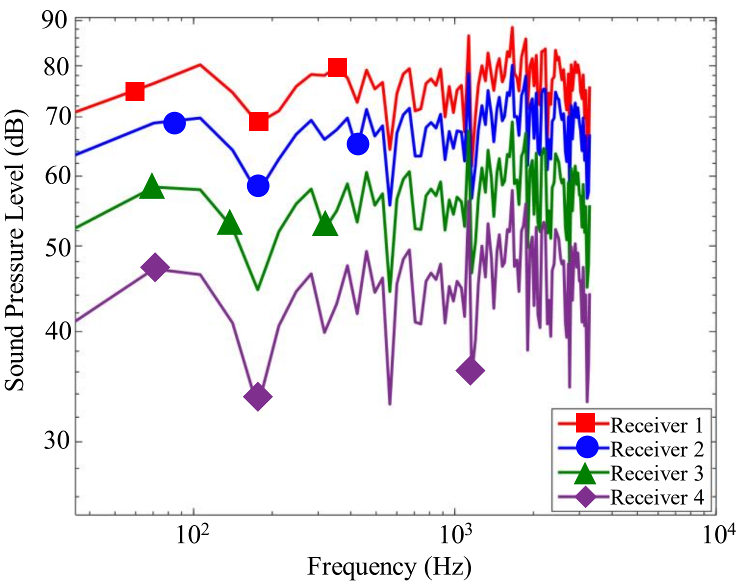

Figure 13. The spectrum of SPL over the frequency range for case 1.

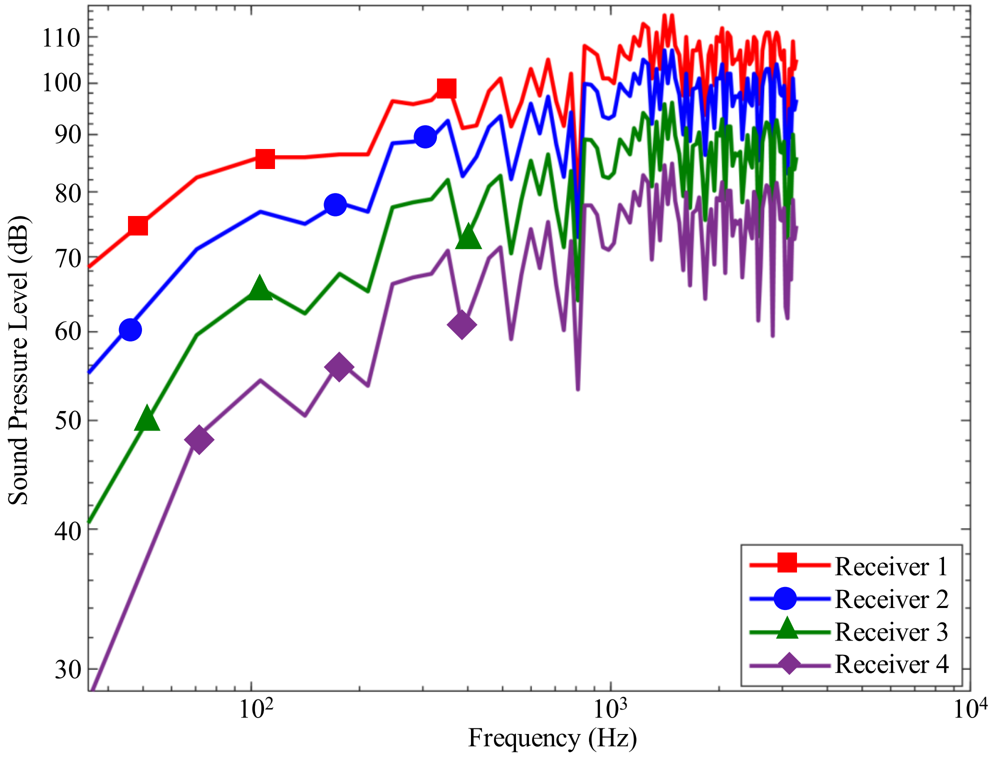

Figure 14. The spectrum of SPL over the frequency range for case 6.

It can be observed from Figure 15 that for case 6, the overall SPL is higher in comparison to case 1 by 15.06% at Receiver 1 to 17.83% at Receiver 4. The average increase in the overall Sound Pressure Level (SPL) is 21.23 dB between these two extreme cases.

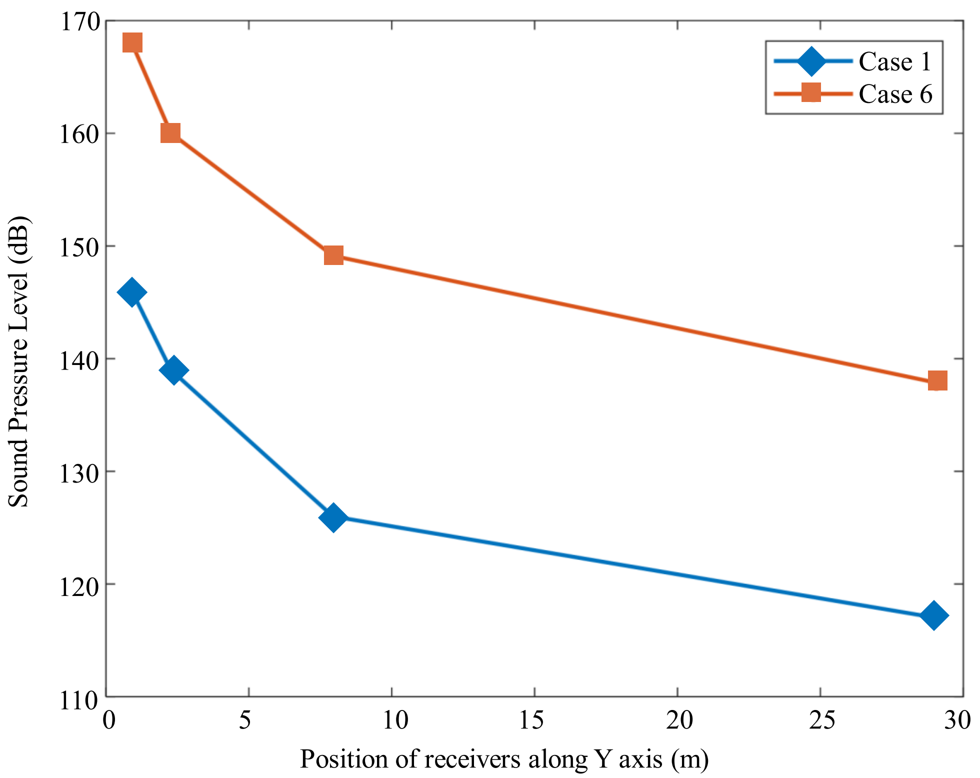

Figure 15. Overall SPLs at various receiver positions.

From the literature [28], it is observed that the difference between non-cavitating and cavitating conditions in terms of the overall SPLs is comparable within the range of 10 to 30 dB. Also, the decreasing trend in this plot is attributed to the phenomenon of attenuation of sound waves occurring as the distance of the receiver increases from the noise source. The acoustic simulations are also under consideration in future like the studies performed by Bagheri et al. [29]. The effects of the hydrophobic silicone fouling-release coating, IS700, on a five-blade propeller were examined by Bagheri et al. They observed that in low-frequency areas in particular, the IS700 coating can reduce noise levels by 2–5 dB under non-cavitation, cavitation inception, and cavitation development situations. The noise reduction rate was lower during fully developed cavitation compared to cavitation inception and non-cavitation situations.

CONCLUSION

The hydrodynamic performance characteristics and acoustic characteristics of an *INSEAN* E779A propeller are studied using CFD software under various operating conditions. The simulations were performed as a transient multiphase phenomenon, and the visualization of the vapor volume was performed to determine the location and extent of cavitating bubbles on the propeller surface. The validation of various open water characteristics was performed, and the influence of the cavitation number on those parameters was identified. Finally, the acoustic simulations are performed to determine the overall SPLs on the propeller surface. Other key findings are listed as follows:

1. R. error % is less than 10% for K_Q and less than 15% for K_T and η. Overall, the simulation results are in the acceptable ranges.
2. The distribution of vapor volume fraction and velocity magnitudes are quantified for various cases and the trend observed is as expected theoretically.
3. The vapor volume fraction distribution and distribution of velocity is determined at 0.7R for all the cases considered. For case 6, at +0.02215 m from the reference line, the vapor volume was 72%, and velocity magnitude of flow had its peak at +0.041596 m with a value of 42.5 m/s.
4. The overall SPL for case 6 (J = 0.55, σ = 0.80) is higher than case 1 (J = 0.91, σ = 4.50) by 15.06% at Receiver 1. This is because the extent of cavitation varies widely in both cases, with the first case showing the maximum cavitating area as observed from the visualization plots. All the receivers follow the same trend, with Receiver 4 showing a variation of 17.83%.
5. Considering the two extreme cases, the average increase in the overall Sound Pressure Level (SPL) is 21.23 dB, with case 6 (J = 0.55, σ = 0.80) developing a much higher noise level. The reason is the high cavitation on the propeller blade surface operating under this particular condition.

The future works involves the consideration of numerical simulations involving fluid-structure interaction where the composite material-based propellers [30] would be considered. Also, the analysis could be performed by considering suitable polymer materials [31] as cavitation resistant coatings so that it would be vital for the experimental view point.

Nomenclature

K_T	Thrust coefficient	--
K_Q	Torque coefficient	--
η	Propeller open water efficiency	--
J	Advance coefficient	--
n	Propeller rotating speed	[rpm]
T	Thrust force	[N]
Q	Torque	[Nm]
D	Propeller diameter	[m]
R	Propeller radius	[m]

P_∞	Free stream pressure	[Pa]
P_v	Vapor pressure	[Pa]
σ	Cavitation number	--
V_a	Advance velocity	[m/s]
SPLs	Sound Pressure Levels	[dB]
CFD	Computational Fluid Dynamics	--

Declaration of Interest

The authors have reported no potential conflict of interest.

Acknowledgement

The authors are thankful to Dr. K. Ajith Kumar, Outstanding Scientist, Director, Naval Physical and Oceanographic Laboratory (NPOL) for giving the facility and encouragement. The first author is thankful to MHRD for providing the fellowship to carry out the research work.

REFERENCES

1. Barnaby SW. On the formation of cavities in water by screw propellers at high speeds. *Journal of the American Society for Naval Engineers*. 1897 Nov;9(4):678-83.
2. Ross, D., & Kuperman, W. A. Mechanics of Underwater Noise. *The Journal of the Acoustical Society of America*. 1989, 86(4), 1626–1626.
3. Sasajima T, Nakamura N, Oshima A. Model and full-scale measurements of propeller cavitation noise on an oceanographic research ship with two different types of screw propeller. *In Shipboard Acoustics: Proceedings of the 2nd International Symposium on Shipboard Acoustics ISSA'86*, The Hague, The Netherlands, October 7–9, 1986 1986 (pp. 63-74). Springer Netherlands.
4. Salvatore F, Testa C, Ianniello S, Pereira F. Theoretical modelling of unsteady cavitation and induced noise. *In Proceedings of CAV 2006 Symposium*, Wageningen, The Netherlands 2006 Sep.
5. Chang B. Application of CFD to P4119 Propeller. *In 22nd ITTC Propeller RANS/Panel Method Workshop*, France 1998 Apr.
6. Sezen S, Atlar M, Fitzsimmons P. Prediction of cavitating propeller underwater radiated noise using RANS & DES-based hybrid method. *Ships and Offshore Structures*. 2021 Aug 18;16(sup1):93-105.
7. Salvatore F, Greco L, Calcagni D. Computational analysis of marine propeller performance and cavitation by using an inviscid-flow BEM model. *In Second International Symposium on Marine Propulsors, (SMP2011)*, Hamburg, Germany 2011 Jun 15.
8. Pan G, Lu L, Sahoo PK. Numerical simulation of unsteady cavitating flows of pumpjet propulsor. *Ships and Offshore Structures*. 2016 Jan 2;11(1):64-74.
9. Pereira F, Salvatore F, Di Felice F. Measurement and modeling of propeller cavitation in uniform inflow. *J. Fluids Eng*. 2004 Jul 1;126(4):671-9.
10. Sperling, L. H. Sound and Vibration Damping with Polymers. *In ACS Symposium Series*. American Chemical Society, 1990, 5–22.
11. Li, B., Zhou, H., & Huang, G. A novel impedance matching material derived from polymer micro-particles. *In Journal of Materials Science*, 2006, 42(1), 199–206.
12. Qian C, Li Y. Review on multi-scale structural design of submarine stealth composite. *In Proceedings of the 2017 2nd International Conference on Architectural Engineering and New Materials*, Guangzhou, China 2017 Feb (pp. 25-26).
13. Jung, K., Yoon, S. W., Cho, K. Y., & Park, J. Acoustic properties of nitrile butadiene rubber for underwater applications. *In Journal of Applied Polymer Science*. 2002. 85(13), 2764–2771.
14. Gu, B.-E., Huang, C.-Y., Shen, T.-H., & Lee, Y.-L. Effects of multiwall carbon nanotube addition on the corrosion resistance and underwater acoustic absorption properties of polyurethane coatings. *In Progress in Organic Coatings*. 2018. 121, 226–235.

15. J. C. F. Pereira and A. Sequeira. Propeller-flow predictions using turbulent vorticity-confinement, *V European Conference on Computational Fluid Dynamics, ECCOMAS CFD 2010*; Lisbon, Portugal. 2010.
16. Schnerr GH, Sauer J. Physical and numerical modeling of unsteady cavitation dynamics. *In Fourth international conference on multiphase flow* 2001 May 27 (Vol. 1, pp. 1-12). New Orleans, LO, USA: ICMF New Orleans.
17. M. Maksoud, Numerical and experimental study of cavitation behaviour of a propeller, Hamburg, Germany: *STG Sprechtag Kavitation*; 2003.
18. Watanabe T, Kawamura T, Takekoshi Y, Maeda M, Rhee SH. Simulation of steady and unsteady cavitation on a marine propeller using a RANS CFD code. *In Proceedings of The Fifth International Symposium on Cavitation (Cav 2003 Nov 1)*.
19. Williams, J. E. F., & Hawkings, D. L. Sound generation by turbulence and surfaces in arbitrary motion. *Philosophical Transactions of the Royal Society of London*. 1969, 264(1151), 321–342.
20. Lighthill, Sir & Thompson, John. Proceedings of the royal society, A. *Proceedings of the Royal Society*. 1986. A 407. 35-50.
21. Seol H, Jung B, Suh JC, Lee S. Prediction of non-cavitating underwater propeller noise. *Journal of sound and Vibration*. 2002 Oct 10;257(1):131-56.
22. Seol, H., Suh, J., & Lee, S. Development of hybrid method for the prediction of underwater propeller noise. *Journal of Sound and Vibration*. 2005, 288(1–2), 345–360.
23. Bagheri, M. R., Seif, M. S., Mehdigholi, H., & Yaakob, O. Analysis of noise behaviour for marine propellers under cavitating and non-cavitating conditions. *Ships and Offshore Structures*. 2015, 12(1), 1–8.
24. Pan, Y., & Zhang, H. Numerical prediction of marine propeller noise in non-uniform inflow. *China Ocean Engineering*. 2013, 27(1), 33–42.
25. Ansys, Inc. *ANSYS CFX-Solver Theory Guide Release 2020-R1*. Canonsburg, PA, USA: ANSYS, Inc.; 2020.
26. Karuppiah G, Kuttalam KC, Palaniappan M, Santulli C, Palanisamy S. Multiobjective optimization of fabrication parameters of jute fiber/polyester composites with egg shell powder and nanoclay filler. *Molecules*. 2020 Nov 27;25(23):5579.
27. Sivasubramanian P, Mayandi K, Santulli C, Alavudeen A, Rajini N. Effect of fiber length on curing and mechanical behavior of pineapple leaf fiber (PALF) reinforced natural rubber composites. *Journal of Natural Fibers*. 2022 Nov 2;19(11):4326-37.
28. Sharma, S. D., Mani, K. V., & Arakeri, V. Cavitation noise studies on marine propellers. *Journal of Sound and Vibration*. 1990, 138(2), 255–28.
29. Bagheri M R, Seif M S, Mehdigholi H. An experimental study on the effect of IS700 coating on the cavitation inception and development, and noise reduction of a marine propeller. *J Appl Mech Eng*, 2017, 6(3): 1000267.
30. Santulli C, Palanisamy S, Kalimuthu M. Pineapple fibers, their composites and applications. In *Plant Fibers, their Composites, and Applications* 2022 Jan 1 (pp. 323-346). Woodhead Publishing.
31. Karuppiah G, Kuttalam KC, Ayrilmis N, Nagarajan R, Devi MI, Palanisamy S, Santulli C. Tribological analysis of jute/coir polyester composites filled with eggshell powder (ESP) or nanoclay (NC) using grey rational method. *Fibers*. 2022 Jul 12;10(7):60.

